Journal of Nuclear Materials 438 (2013) S809–S813

Contents lists available at SciVerse ScienceDirect

Journal of Nuclear Materials

journal homepage: www.elsevier.com/locate/jnucmat

Integrated self-consistent analysis of NSTX performance during normal operation and disruptions

Valeryi Sizyuk *,[1], Ahmed Hassanein

Center for Materials Under Extreme Environment, School of Nuclear Engineering, Purdue University, West Lafayette, IN 47907, USA

ARTICLE INFO

Article history:
Available online 16 January 2013

ABSTRACT

A fundamental issue in tokamak operation related to power exhaust is the understanding of heat and particle transport from core plasma into scrape-off-layer (SOL) and to plasma facing materials during plasma instabilities. We enhanced our models and upgraded HEIGHTS package using adaptive mesh refinement (AMR) to fit reactor walls arbitrary geometry and study/implementing nanoscale surface processes. A five-layer quadtree refinement scheme is used for simulation of the entire SOL plasma evolution and the extra refinement mesh (~0.5 μm) allowed detail calculations of subsurface particle implantation, divertor hydrodynamic evolution, and erosion processes. Using NSTX actual geometry and magnetic field structure we modeled in full 3D the evolution of escaped core plasma particles starting at core border, gyration and scatterings in SOL, and deposition into plasma facing components. The characteristics of the escaped particles determined the energy source and boundary conditions for edge plasma MHD evolution and the resulting damage.

Published by Elsevier B.V.

1. Introduction

Edge plasma evolution plays major role in tokamak plasma confinement and determines/control the High-confinement mode (H-mode) operation. Experiments show the complex character of the edge plasma interaction with tokamak components and as a result the complex self-consistent behavior of plasma in the entire SOL. The edge plasma drift and contact with plasma facing components (PFCs) results in redistribution of D-T plasma and components material impurities, affects toroidal plasma motion, and redistributes energy load. Plasma instabilities occurs in various forms such as hard disruptions, which include both thermal and current quench, edge localized modes (ELMs), runaway electrons, and vertical displacement events (VDEs). Most recent experimental and theoretical studies of PFCs erosion were performed for local areas of tokamak PFCs [1–4]. Our previous simulations [2] showed that the physical processes involved are highly intercorrelated and for accurate understanding, self-consistent integrated models for the entire SOL area should be implemented. The integrated models should combine micro- and macro-scale physical processes within the divertor nearby areas and the SOL edge plasma. The energy load emitted from core plasma particles into divertor/wall surface and the resulting heat conduction, melting, and vaporization of plasma facing materials should be considered in detail in which the MHD vapor expansion and evolution is controlled by the heating of the escaped core particles. Magnetic diffusion, heat conduction, and photon radiation transport should be calculated in fine details in the developed vapor edge plasma. Our simulation showed that surface erosion is a complex self-consistent problem where the local spatial profile is strongly coupled through vapor MHD and photon transport processes. The escaped core plasma source initiates multi-component interplay of various related edge processes. The characteristics of nearby Separatrix area have significant influence on energy and particles confinement time and consequently on the temperature and density of core plasma.

In our foregoing study [5] we simulated the evolution of edge plasma during the normal and disruptive operation of tokamak devices in localized areas of the SOL using our HEIGHTS (High Energy Interaction with General Heterogeneous Target Systems) computer simulation package containing various integrated models [6–8]. We included in our models five main parts: Monte Carlo block of disrupting plasma particles interaction with solid and plasma matter; MHD block of plasma evolution taking into account magnetic field diffusion; heat conduction and vaporization block for plasma facing components; heat conduction block for vapor and plasma; and Monte Carlo radiation transport block. The radiation transport block is based on the optical data calculated by HEIGHTS atomic physics package [9]. Direct expansion of the computational domain to include the entire SOL leads to significant calculations overload and to the problem of multiscale description of the complex various design components. The size of the fusion device is measured in meters, accurate MHD calculations require cell sizes of 100–200 μm, and detail surface erosion simulation requires mesh

* Corresponding author. Address: Purdue University, 400 Central Drive, West Lafayette, IN 47907, USA.
E-mail address: vsizyuk@purdue.edu (V. Sizyuk).
[1] Presenting author.

0022-3115/$ - see front matter Published by Elsevier B.V.
http://dx.doi.org/10.1016/j.jnucmat.2013.01.175

discretization level of cell size less than 0.5 μm. To avoid the described limitations in edge plasma modeling and to adopt the multiscale approach of the integrated physical and mathematical models, we developed unstructured adaptive mesh approach in computational domain and reconstructed all integrated physical processes in the upgraded numerical methods and computational algorithms of HEIGHTS package. A five-layer quadtree refinement scheme [10] is used for simulation of the entire SOL plasma evolution and the extra refinement (~0.5 μm) allowed calculations of subsurface particle implantation, heat deposition, and erosion processes. Using actual NSTX geometry and magnetic field structure we simulated in full 3D the evolution of escaped core plasma particles: starting at core border, gyration and scatterings in SOL, and penetration and deposition into PFCs. The escaped core particles determined the initial energy source and boundary conditions for the edge plasma MHD evolution. The plasma magnetic diffusion, heat conduction, and radiation transport are also considered in the quadtree grid hierarchy.

2. Mathematical and physical models

The upgraded HEIGHTS models now include six main parts: Monte Carlo block of the core escaping plasma particles; Monte Carlo block for plasma particles gyration, drift, and interactions with solid/liquid and plasma matter in magnetic field of any configuration; heat conduction and vaporization block for thermal evolution and vaporization of divertor material; MHD block of near divertor area plasma evolution; heat conduction block for vapor and plasma; and radiation transport block based on weighted Monte Carlo methods. All blocks were adapted for the quadtree adaptive mesh [10] and applied to the NSTX design shown in Fig. 1. Here we assumed r -axis as radial, φ -axis as toroidal, and z-axis as the poloidal directions. In the cylindrical coordinate system $S(r,\varphi,z)$, the full MHD equations set [2] can be presented in matrix form where full description of the MHD cell state includes eight variables: $\mathbf{U}(/\rho,\rho v_r,\rho v_\varphi,\rho v_z,e_h,B_r,B_\varphi,B_z/)$

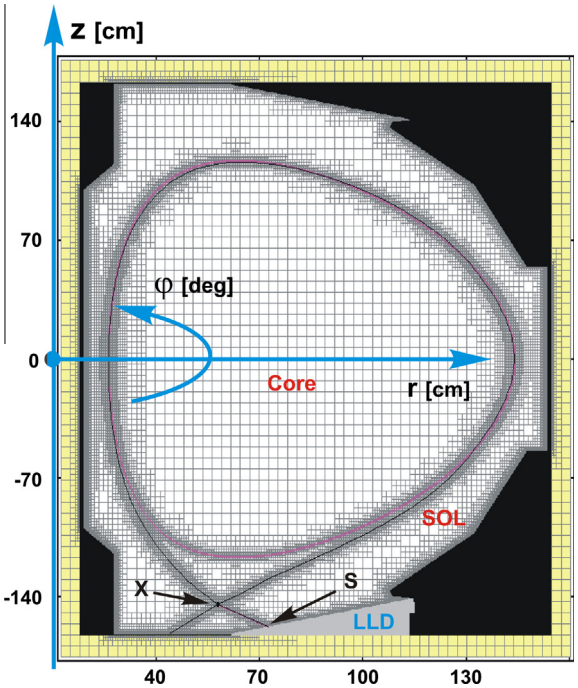

Fig. 1. Schematic of NSTX liquid lithium divertor and orientation of coordinate system used in the simulation [11]: 1 – particles source; 2 – device surface; and 3 – initiated divertor plasma.

$$\frac{\partial \mathbf{U}}{\partial t}+\frac{1}{r}\frac{\partial}{\partial r}[r\mathbf{F}(\mathbf{U})]+\frac{\partial \mathbf{P}(\mathbf{U})}{\partial r}+\frac{\partial \mathbf{G}(\mathbf{U})}{\partial z}=\Omega. \tag{1}$$

Here the convective fluxes **F**, **P**, and **G** are given as

$$\mathbf{F}(\mathbf{U})=\begin{bmatrix}\rho v_r\\ \rho v_r^2-B_r^2/4\pi\\ \rho v_\varphi v_r-B_\varphi B_r/4\pi\\ \rho v_z v_r-B_z B_r/4\pi\\ v_r(e_h+p_h)\\ 0\\ 0\\ v_r B_z-B_r v_z\end{bmatrix},\quad \mathbf{P}(\mathbf{U})=\begin{bmatrix}0\\ p_t\\ 0\\ 0\\ 0\\ 0\\ v_r B_\varphi-B_r v_\varphi\\ 0\end{bmatrix},$$

$$\mathbf{G}(\mathbf{U})=\begin{bmatrix}\rho v_z\\ \rho v_r v_z-B_r B_z/4\pi\\ \rho v_\varphi v_z-B_\varphi B_z/4\pi\\ \rho v_z^2+p_t-B_z^2/4\pi\\ v_z(e_h+p_h)\\ v_z B_r-B_z v_r\\ v_z B_\varphi-B_z v_\varphi\\ 0\end{bmatrix}, \tag{2}$$

The dissipation processes Q are shown in the matrix Ω:

$$\Omega=\begin{bmatrix}Q_{vap}\\ \rho v_\varphi^2/r-B_\varphi^2/4\pi r-B_r(\partial B_r/r\partial r+\partial B_z/\partial z)/4\pi\\ \rho v_r v_\varphi/r-B_r B_\varphi/4\pi r-B_\varphi(\partial B_r/r\partial r+\partial B_z/\partial z)/4\pi\\ -B_z(\partial B_r/r\partial r+\partial B_z/\partial z)/4\pi\\ Q_{th}+Q_{vap}+Q_J+Q_{rad}+Q_{imp}\\ -v_r(\partial B_r/r\partial r+\partial B_z/\partial z)+Q_{rdiff}\\ -v_\varphi(\partial B_r/r\partial r+\partial B_z/\partial z)\\ -v_z(\partial B_r/r\partial r+\partial B_z/\partial z)+Q_{zdiff}\end{bmatrix}. \tag{3}$$

Here, ρ is density; $\mathbf{v}(v_r,v_\varphi,v_z)$ is velocity; $\mathbf{B}(B_r,B_\varphi,B_z)$ is magnetic field; $e_h=e_{in}+e_{kin}$ is the hydrodynamic energy, which includes the internal and kinetic energy. Pressure has hydrodynamic and magnetic parts: $p_t=p_h+(B^2/8\pi\mu)$. The dissipative processes are presented here as the source terms: Q_J is the Joule heat term, Q_{th} is the heat conduction term; Q_{vap} is the surface vaporization term; Q_{diff} is the magnetic diffusion term; Q_{imp} is the core plasma energy deposition; and Q_{rad} is the radiation transport. We calculated these terms separately by using the splitting method in similarity to the structured mesh model [12]. Because plasma parameters are assumed invariable along the divertor surface in toroidal direction we take into account zero derivatives of all variables in the φ-direction. We used four levels of refinement for accurate description of plasma evolution parameters near wall surfaces, Separatrix, and the X-point. Utilizing the new unstructured mesh requires reimplementation of all mathematical models and numerical methods starting from the MHD and finishing at the dissipative processes. A general schematic of the interfaces between cells in new mesh is shown in Fig. 2. In terms of the finite volume approach, the general MHD equation set for the coordinates system corresponding to Fig. 2 was transformed as:

$$\mathbf{U}^{n+1}=\mathbf{U}^n-\frac{\Delta t^n}{V}\left(\sum_{i=1}^{N^R}\mathbf{F}_i^R S_i^R-\sum_{i=1}^{N^L}\mathbf{F}_i^L S_i^L+\sum_{i=1}^{N^T}\mathbf{G}_i^T S_i^T-\sum_{i=1}^{N^B}\mathbf{G}_i^B S_i^B\right)-\\ -\Delta t^n\left(\sum_{i=1}^{N^R}\mathbf{P}_i^R\frac{S_i^R}{V+\Delta V}-\sum_{i=1}^{N^L}\mathbf{P}_i^L\frac{S_i^L}{V-\Delta V}-\Omega\right), \tag{4}$$

where $V=\pi(r_R^2-r_L^2)\,\Delta z$ is cell volume and $\Delta V=\pi\Delta r^2\Delta z$ is correction of geometrical cell volume due to the cylindrical coordinate system and indexes *L, R, B, T* correspond to the left, right, bottom, and top cell borders. We constructed the explicit total variation

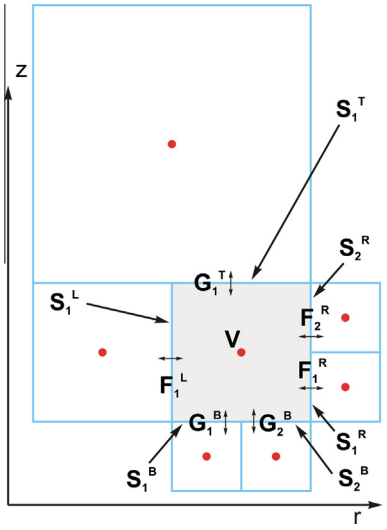

Fig. 2. Schematic of cell interfaces and border fluxes in quadtree AMR.

diminishing numerical algorithm in Lax–Friedrich formulation by calculating the convective fluxes from the $\mathbf{U}^n$ field following the method described in Ref. [13]. As in our previous work [2], [5], we used the numerical errors correction (see Eq. (3)) based on the local magnetic field divergence. The dissipative processes were described by calculating cell border fluxes from the $\mathbf{U}^{n+1}$ field and consequent assembly of the linear equations system based on Eq. (4). Here the flux **P** is equal zero for dissipative processes. The computational blocks of the core plasma impact and radiation transport and were previously developed using Monte Carlo simulators of particles motion in arbitrary 3D geometry [2,5,6].

3. Simulation results

We modeled the escaping of ELM and disruption particles into the SOL area starting from the core plasma border of the tokamak. We assumed a uniform distribution of particles starting along the core border. The total energy $Q = 74$ kJ was partitioned between the escaping particles to describe the plasma impact during $t = 0.1$ ms at plasma temperature $T = 250$ eV. The plasma impact fluxes were calculated from the statistical accumulation of the 3D particles motion: toroidal rotation, poloidal drift, and gyration along the magnetic field lines as illustrated in Fig. 3. The initial distribution of plasma impact along the lithium divertor corresponds to the previous simulation calculated assuming local interaction where only limited divertor nearby space was included into domain [5]. In the localized scheme, the impact particles were artificially distributed exponentially on domain border. The initial magnetic field (shown in Fig. 4) was reconstructed from the equilibrium EQDSK file for NSTX with liquid lithium divertor (LLD) module [14]. The incident plasma energy is deposited inside the lithium divertor of up to 10 μm depth. The maximum deposition is located at 1 μm below the surface. The net heat load and vaporization rate of liquid lithium divertor depends on impact duration, impact energy, and characteristics of the divertor plasma hydrodynamic evolution. The expansion of computation domain to include the entire SOL area showed the more complex self-consistent character of the divertor plasma evolution that corresponds to recent experimental observations [15,1]. Opposite to previous localized simulations, two divertors energy load were interconnected through the toroidally drifting escaped core particles: the ions and electrons can change gyration pitch and drifting status (trapped particle–passing particle) due to interaction with the

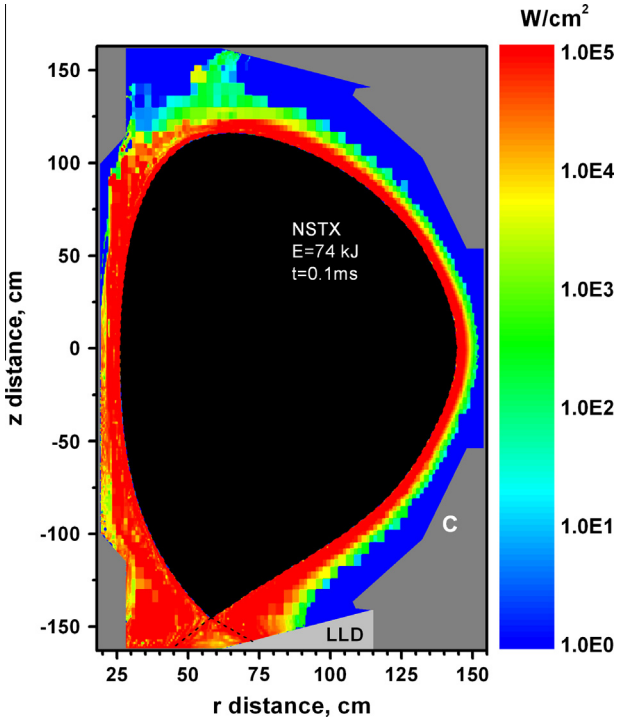

Fig. 3. Initial core plasma impact fluxes during the disruption of $Q = 74$ kJ and $t = 0.1$ ms.

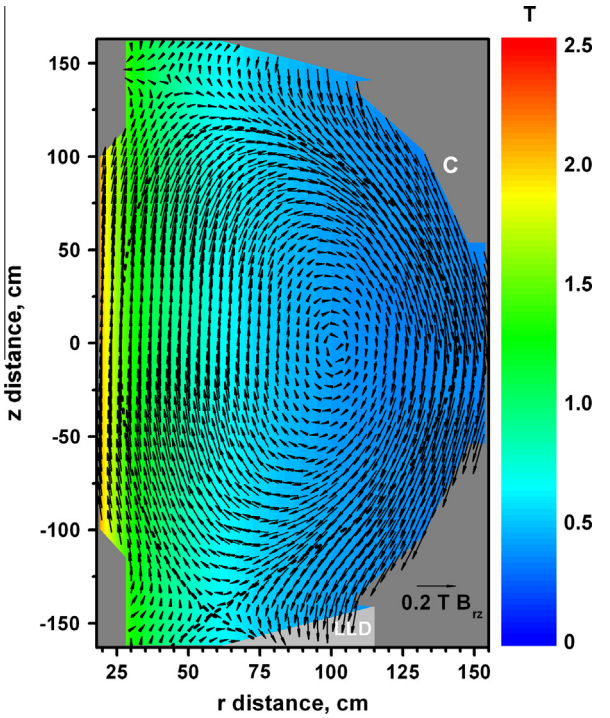

Fig. 4. Initial magnetic field reconstructed using EQDSK file [14].

divertor plasma. A part of the escaped particles roams between inner and outer divertors around the abandoned core. After the plasma impact start, the drifting particles arrive at the divertor strike-point location and initiates Li vaporization and plasma cloud formation. Because of evolving plasma-shielding effect, the impact power at the strike point is decreased and the peak of energy

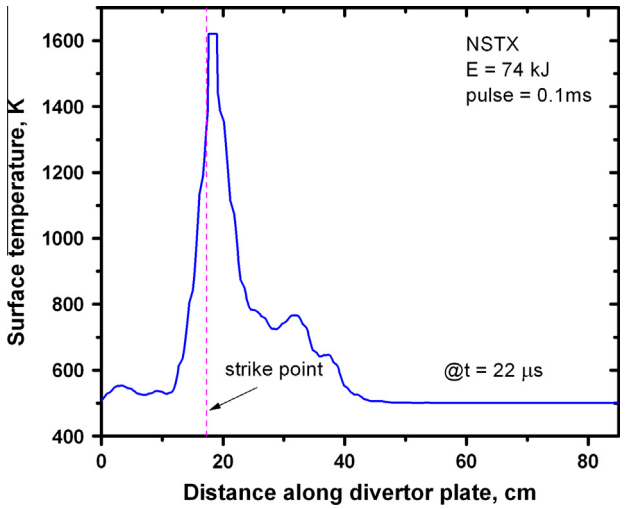

Fig. 5. LLD surface temperature at $t = 22$ μs during disruption of $Q = 74$ kJ and $t = 0.1$ ms.

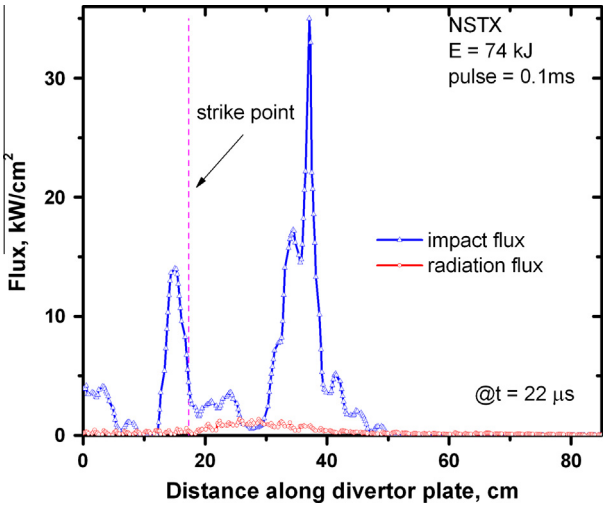

Fig. 6. Disruption energy deposition fluxes at LLD surface at $t = 22$ μs .

deposition changes location along the lithium surface. As result, the lithium surface temperature spatial profile varies during the impact time. Fig. 5 shows the surface temperature at time $t = 22$ μs. Initially, the vaporization area is located at the strike point but plasma shielding effect decreases the impact flux at this location as shown in Fig. 6. A comparison between Figs. 5 and 6 explains the formation of the additional temperature peaks near the main maximum strike point. The maximum vapor plasma temperature is around 16 eV and is located above the liquid divertor strike point as shown in Fig. 7. The motion of the plasma density follows the magnetic field lines from the strike point to X-point and into the SOL zone along device walls. The calculated low radiation fluxes of up to 2 kW/cm^2 for the disruption energy of $Q = 74$ kJ in comparison to the initial plasma particles impact fluxes will not cause serious damage to nearby components in comparison to ITER ELM and disruption conditions [2]. The calculated surface temperature at the internal carbon divertor strike point was $T \sim 1500$ K. Because the MHD evolution requires sometime, the role of the evolved vapor plasma increases with the core plasma impact elongation [5]. The plasma cloud requires sufficient time for motion and expansion in SOL zone. Investigation of Li vaporization profiles, Li plasma cloud motion in SOL, and plasma-shielding effects as

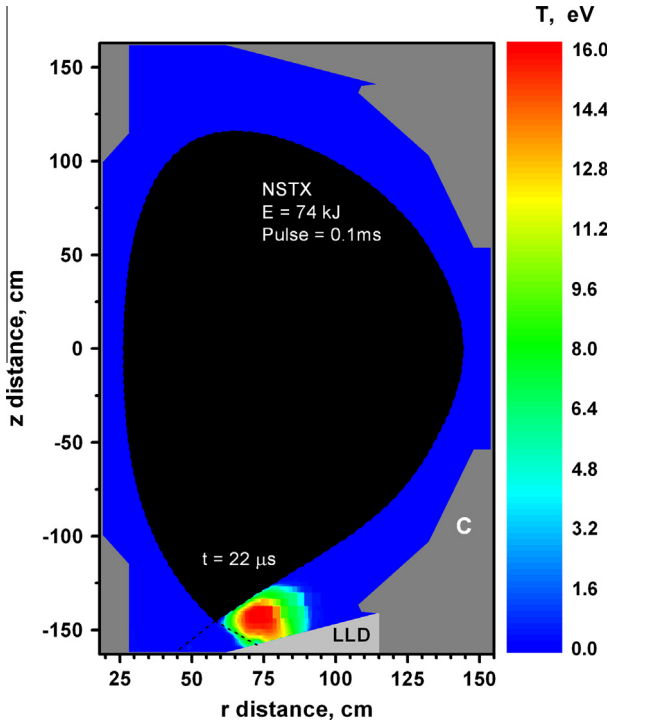

Fig. 7. Plasma temperature at $t = 22$ μs during disruption of $Q = 74$ kJ and $t = 0.1$ ms.

function of various NSTX ELM and disruption parameters are currently being considered in our simulation.

4. Conclusion

The upgraded HEIGHTS package proved the necessity of integrating edge plasma transport in the expanded entire SOL domain and the accurate assessment of impurities drift with integration of nanoscale processes on plasma facing and nearby component surfaces. We enhanced our models and numerical methods using adaptive mesh refinement (AMR) for fitting any arbitrary geometry of device walls and implementing nanoscale surface processes. A five-layer quadtree refinement scheme is used for the simulation of entire SOL plasma evolution and the extra refinement (~0.5 μm) allowed accurate calculations of subsurface particle implantation, heat deposition, and erosion processes. Using NSTX actual geometry and magnetic field structure we simulated in full 3D the evolution of escaped core plasma particles, i.e., starting from core border, gyration and scatterings in SOL, and then penetration into device components. The escaped particles determined the initial energy source and boundary conditions for the edge plasma MHD evolution. The plasma magnetic diffusion, heat conduction, and radiation transport are also implemented using the quadtree grid hierarchy. The lithium divertor heat load, divertor surface erosion profile, and potential lithium impurities drift were calculated for the coupled system of the inner and outer divertors interconnected through the SOL. The detailed simulation results of the inner-outer divertor system are currently under preparation now for the comprehensive publications.

Acknowledgements

This work is supported by the US Department of Energy, Office of Fusion Energy Sciences.

References

[1] T.K. Gray et al., J. Nucl. Mater. 415 (2011) S360.
[2] V. Sizyuk, A. Hassanein, Nucl. Fusion 50 (2010) 115004.
[3] J.W. Coenen et al., Nucl. Fusion 51 (2011) 083008.
[4] A. Kreter et al., J. Nucl. Mater. 390–391 (2009) 38.
[5] V. Sizyuk, A. Hassanein, J. Nucl. Mater. 415 (2011) S881.
[6] V. Sizyuk, A. Hassanein, Nucl. Fusion 49 (2009) 095003.
[7] A. Hassanein et al., Fusion Eng. Des. 69 (2003) 781.
[8] A. Hassanein, I. Konkashbaev, J. Nucl. Mater. 313–316 (2003) 664.
[9] V. Tolkach, V. Morozov, A. Hassanein, Development of comprehensive models for opacities and radiation transport for IFE systems, Argonne National Laboratory Report ANL-ET/02-23, Argonne, IL, 2002.
[10] W. Lee, A. Borthwick, P. Taylor, J. Comp. Phys. 230 (2011) 4848.
[11] B. Nelson, P. Fogarty, Engineering configuration options for flowing lithium surfaces in NSTX, APEX Electronic meeting, August 24 2000.
[12] G.V. Miloshevsky et al., J. Comp. Phys. 212 (2006) 25.
[13] R.J. Leveque, Finite Volume Methods for Hyperbolic Problems, Cambridge University Press, Cambridge, 2002.
[14] D.P. Stotler et al., Contrib. Plasma Phys. 50 (2010) 368.
[15] J.-W. Ahn et al., J. Nucl. Mater. 415 (2011) S918.